Pyramidal Refinement of Lucas – Kanade Optical Flow based Tracking of Peripheral Air Embolism in OCT Contrast Imaging

Kausik Basak[1], Manjunatha M[1], Pranab Kumar Dutta[1, 2]
[1]School of Medical Science and Technology
[2]Department of Electrical Engineering
Indian Institute of Technology Kharagpur
Kharagpur 721 302, India

ABSTRACT
Air embolism often causes severe consequences in patients, in which several cases need fast treatment at the earlier stage. This paper proposes a computerized approach for detection as well as estimation of motion trajectory of air emboli using OCT contrast imaging technique. Due to change in optical properties, speckle pattern changes from fluid to air bubble and so does the speckle pattern on the image plane. This phenomenon helps to track the air bubble due to change in brightness pattern over a sequence of images. A top-down approach has been demonstrated from the image acquisition to the application of different image processing algorithms. Segmentation of the embolus has been carried out primarily by selecting seed contour through anisotropic diffusion (AD) technique and then implementation of a snake based active contour (AC) method. Both the techniques reduce the manual labour and computational time, thereby substantially increasing the segmentation accuracy (92% - 94%). Besides, pyramidal construction of the Lucas – Kanade optical flow precisely optimizes the flow velocities of air bubble and also increases larger motion tracking ability. Hence, the proposed technique can becoming an assisting tool to the clinician for early detection of air embolism and tracking the air bubble through microcirculation.

General Terms
Image Processing, Optical Coherence Tomography, Medical Imaging, Computer Vision.

Keywords
Optical coherence tomography (OCT), active contour, air embolism, image segmentation, optical flow, least square estimation.

1. INTRODUCTION
Air embolism can become a life threatening disorder for which a computerized detection and diagnosis is of major importance. It occurs when an air bubble enters into the circulation, travels through vascular system and creates a blockage in normal blood flow pathway to a particular region far from its origin [1, 2]. This results in damage of the tissue structure as it restricts further blood supply to the cells in that particular region, for which the cells die due to lack of oxygen and nutrients. A survey in USA leads to a figure of approximately 20,000 patients counted due to air embolism, in which many of them required fast treatment in the earlier stage [1]. Basically, due to bifurcation in the blood channel, these air emboli stop at the narrower regions. Sometimes, the results turned into a severe heart attack and stroke when an air bubble clogs in the brain circulation and coronary artery respectively [1, 2]. Air embolism can be of two types; venous air embolism (pulmonary air embolism) refers to the situation when an air bubble travels through the right side of the heart to the lung and creates a sudden blockage in blood flow of the artery that feeds the lungs. This can be a cause of respiratory distress and hypoxia [3, 5–7]. According to the study of Bouma et al., pulmonary embolism (PE) has been found in one of 500 people across USA, in which approximately 11% cases has been reached to death whereas untreated PE is observed to have a high mortality rate of about 30% [5]. Other hand, arterial air embolism causes ischemia in different organs of the body by blocking the area fed by the artery. It can cause a stroke when it lands in the brain circulation. Often, it also hinders the blood flow through coronary artery, thereby causing of ischemic heart attack [1]. That is why; determining the flow trajectory of air emboli within a vasculature is of major importance in diagnosing different pathological conditions.

Optical flow can deliver significant potential in this context for tracking the air bubble while flowing through the channel. Motion estimation is one of the important aspects while considering the flow of gray values on the image plane in time varying images. Optical flow can provide an apparent velocity distribution of movement of brightness pattern over a sequence of images [8]. Different procedures have been approached in this regard; differential methods, region based matching, energy based methods and other follows feature based optimization of optical flow over time varying images [9]. This paper mainly focuses on the gradient based calculation of gray level values. Determining the motion field of the air bubble is highly regulated by the degree of accurate estimation of the flow field and the computational time. Some of the techniques of calculating optical flow is affected by the data conservation and spatial coherence, whereas some methods result very precise optical flow but lacks in computational time [10]. Here, pyramidal Lucas – Kanade algorithm is implemented for flow field optimization which comprises least square estimation based error minimization technique. Prior to the optical flow algorithm, air embolus needs to be segmented from the channel. Active contour (AC) is employed for the segmentation of the embolus within microchannel. This work proposes an improved snake based AC implementation by incorporating a grow energy force, thereby moving the contour from the origin of seed contour to

track the boundary [12]. This will substantially reduce computational time. The technique can also facilitate the segmentation of moving emboli over a sequence of images.

1.1 Organization of the Paper

This paper focuses on the optical coherence tomography (OCT) based contrast imaging technique for embolism detection. In the following sections of this paper, active contour (AC) based segmentation is implemented to locate the blockage and to perform the shape analysis of the embolus. Manually selecting the seed point lacks in the context that the boundary should be placed accurately near actual boundary and the process of energy minimization as well as tracking the boundary become time consuming. Here, anisotropic diffusion is utilized to initialize the contour points for AC implementation. Different parameters of AC are optimized and the method is executed over several numbers of successive time frames. This results in the displaced segmented out embolus over the sequence of images. Thereafter, pyramidal Lucas – Kanade based optical flow algorithm is implemented over those images for tracking the velocity trajectory of the air embolus.

2. MATERIALS AND METHODS

2.1 Sample Preparation and Experimental Setup

The overall imaging setup is depicted in figure 1. A swept laser source is tuned across a broad lasing wavelength to illuminate the interferometer. The swept source has a built-in Mach-Zehnder Interferometer (MZI, Thorlabs INT-MZI-1300) that provides the frequency clock for the laser. The depth profile imaging is carried out at tens of kiloheartz repetition rate of the laser. The en-face images are acquired from the CMOS camera channel by incorporating a dichroic mirror into the beam path to reflect the visible light from sample onto the CCD camera. Cross-sectional images which reveal the samples internal structure are captured from the OCT channel. The transverse scan is controlled by the galvo scanning mirrors which determine the frame rate of the OCT imaging.

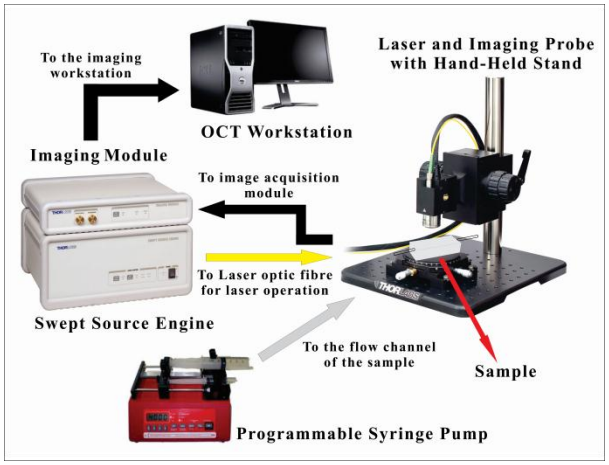

Figure 1. OCT imaging instrumentation

Different geometric flow channels have been prepared in the paraffin blocks. Some are straight channel with constant and inclined depth properties and Y – shaped channel. Inner diameter of which is kept at 2 mm with a depth of 0.5 – 1 mm below the superficial surface. The experiment has been carried out with a Swept Source Optical Coherence Tomography (SS – OCT) machine (ThorLabs) to study the contrast variations due to presence of an air bubble. The sample is placed on the stage capable of both XY and rotational translation. A mixture of saline and red gel ink has been pumped through the channel by a programmable syringe pump (NE – 4000, Newera) at a rate of 400 – 700 microlitre/min for maintaining a suitable velocity range (14 – 18 mm/sec) and contrast variations. The transverse resolution of the imaging module is 15 micron and axial resolution (air/water) is 12/9 micron. The swept source engine is triggered to start the lasing operation. A scanning laser (1325 nm), having an average output power of 10 mW, is directed on the channel for acquiring 2D cross sectional images at a rate of 20 fps and they are transferred to the workstation for image analysis. The images are further used for different image processing applications.

Contrast image of the bubble roughly describes the portion of blockage present in the flow path. Contrast variation arises due to different optical properties of the fluid and the air bubble. Different image processing techniques are employed to segment the contour of the air embolus for tracking its motion field. The overall implementation is illustrated in following sections.

2.2 Embolus Segmentation: Anisotropic Diffusion and Active Contour method

A median filter has been applied first over the raw speckle image to reduce the effect of background noise. This would subsequently blur the AOI also. So, the intensity of AOI has been improved by dithering the image to lowest and highest grey levels. Dithering helps to distinguish foreground from background by transforming the gray image to its binary (black and white) counterpart. Detecting seed contour of the emboli is the first step of segmenting the air bubble present in the channel. This paper focuses on the use of AD filtering to extract the seed contour [15]. The piecewise smoothing has been performed on the original image $I_0(x,y)$ by convolving with a Gaussian filter $G(x,y;t)$ of variance t (scale-space parameter), thereby producing a successive number of more and more blurred images [15]. The parameter of the mask depends on the local content of the original image. The family of blurred images $I(x,y,t)$ can be represented as,

$$I(x,y,t) = I_0(x,y) * G(x,y;t) \tag{1}$$

with initial condition $I(x,y,0) = I_0(x,y)$, the original image. Mathematically, the AD equation can be written as,

$$I_t = div\left(c(x,y,t)\nabla I\right) = c(x,y,t)\Delta I + \nabla c \cdot \nabla I \tag{2}$$

For a constant $c(x,y,t)$, the above diffusion equation becomes isotropic as given by [15],

$$I_t = c\Delta I \tag{3}$$

Let, $E(x,y,t)$ be an estimate of boundary (edge) location having the following properties as:

a) $E(x,y,t) = 0$ within each region.

b) $E(x,y,t) = Ke(x,y,t)$ at each edge point, where, e is the unit vector normal to the edge at the point and K is the local contrast of the edge.

Hence, the conduction coefficient $c(x,y,t)$ can be represented as a function of the estimate as given by,

$$c = g\left(\|E\|\right) \tag{4}$$

where, $g(\mathrm{g})$ has to be a nonnegative, monotonically decreasing function with $g(0)=1$, resulting a smoothed intensity levels within each region without affecting boundaries where the magnitude of *E* is large. Different functions can be used for $g(\mathrm{g})$ for edge detection mechanism [15]. Perona and Malik have shown that the simplest estimate of the edge positions providing excellent results are given by the gradient of the brightness function i.e. $E(x,y,t)=\nabla I(x,y,t)$. So the conduction coefficient can be written as,

$$c(x,y,t) = g\left(\left\|\nabla I(x,y,t)\right\|\right) \tag{5}$$

AD filtering roughly extracts the bubble (embolus) boundary which is further utilized as an initial guess for active contour mechanism.

In the next stage of segmentation, an improved snake based AC technique is implemented for actual bubble segmentation [12]. The goal is to reach for a curve where the weighted sum of internal and external energy will be minimum. Mathematically it can be formulated as,

$$E_{snake} = \int_0^1 \left\{E_{\text{int}}\left(v(s)\right) + E_{ext}\left(v(s)\right)\right\} ds \tag{6}$$

Where, the position of snake is represented by a planar curve $v(s)=(x(s),y(s))$, E_{int} is the internal energy force, used to smooth the boundary during deformation. E_{ext} represents the external energies, pushing the snake towards the desired object. The coordinates of seed contour is transformed into polar form (ρ,θ). Quantization step for the parameters is chosen to be ρ_s and $\theta_s\left(=2\pi/n\right)$ respectively. The contour is now represented with a set of such discrete polar coordinates $v_i=(\rho_i,\theta_i)$ for $i=0,1,2,....,(n-1)$; where angle $\theta_i = i\times\theta_s$. The energy function of this model is given by,

$$E = \sum_{i=0}^{n-1}\left(aE_{cont}\left(v_i\right) + bE_{curv}\left(v_i\right) + cE_{image}\left(v_i\right) + dE_{grow}\left(v_i\right)\right) \tag{7}$$

Dfsdf According to figure 2, for each point v_i for $i=0,1,2,....,(n-1)$, the energies at the points $\Omega_i=\left\{v_i^-, v_i, v_i^+\right\}$ are calculated and v_i is moved to the point with the minimum energy among these three where v_i^- and v_i^+ are the two discrete points adjacent to v_i at the radial direction. This operation is performed iteratively until the number of moved contour points is sufficiently small or the iteration time exceeds a predefined threshold. The energy functions are: E_{cont} is the internal continuity spline energy that helps to maintain the contour to be continuous, E_{curv} is the internal curvature energy for smoothing the periphery, E_{image} is external image force that depends on the image intensity points and E_{grow} represents the external grow energy that helps to expand the contour from the centre towards the boundary. Mathematically they can be formulated as below [12].

$$E_{cont}\left(v_j\right) = \left|\bar{d} - \left|v_j - v_{i-1}\right|\right| + \left|\bar{\rho} - \left|\rho_j - \rho_{i-1}\right|\right| \quad \left(v_j \in \Omega_i\right) \tag{8}$$

where, $\bar{d} = \sum\frac{\left|v_t - v_{t-1}\right|}{n}$ and $\bar{\rho} = \sum\frac{\left|\rho_t - \rho_{t-1}\right|}{n}$

$$E_{curv}\left(v_j\right) = \left|v_{i+1} - 2v_j + v_{i-1}\right|^2 + \left|\rho_{i+1} - 2\rho_j + \rho_{i-1}\right|^2 \quad \left(v_j \in \Omega_i\right) \tag{9}$$

$$E_{image}\left(v_j\right) = \frac{1}{R}\sum_{r=1}^{R} I\left(\rho_j + r\times\rho_s, \theta_j\right) - \frac{1}{R}\sum_{r=1}^{R} I\left(\rho_j - r\times\rho_s, \theta_j\right) \quad \left(v_j \in \Omega_i\right) \tag{10}$$

$$E_{grow}\left(v_j\right) = \begin{cases} e & \text{if } v_j = v_i^+ \text{ and } \left|\bar{I}_{v_j} - \bar{I}_{origin}\right| < T \\ 0 & \text{else} \end{cases} \tag{11}$$

where, $\bar{I}_{v_j} = \frac{1}{k\times k}\sum_{v_i\in\Psi_{v_j}} I\left(v_i\right)$ and $\bar{I}_{origin} = \frac{1}{k\times k}\sum_{v_i\in\Psi_0} I\left(v_i\right)$

Ψ_{v_j} and Ψ_0 are two $k\times k$ (k is an odd number) sub-blocks with centre points at v_i and the centroid of the contour respectively. The energy will decrease at v_i^+ if both the sub-blocks are of same intensity approximately, resulting in an outward movement of the contour. This movement stops while the sub-blocks having different intensities. Threshold *T* determines the range upto which the change in intensity is allowed. *e* is a negative constant, small value of which will limit the algorithm for more shape restrictions where large value of *e* also nullifies the effect of image energy for which the contour can exceed the actual boundary.

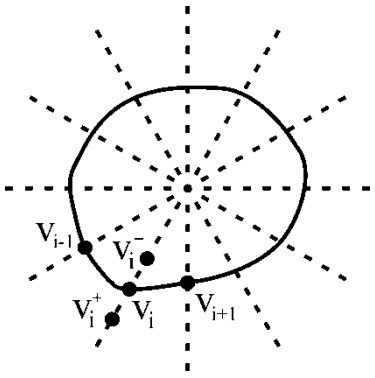

Figure 2. Active contour (snake) in polar coordinate

2.3 Motion Estimation of Embolus: Optical Flow Algorithm

Once the contours of the bubble have been segmented over an image sequences, optical flow can map the three dimensional motion of intensity points into two dimensional image plane. Optical flow is computed assuming the brightness of a particular image point is constant over time (brightness constancy). Let, an image point *(x, y)* is moved to a new

coordinate *(x+uδt, y+vδt)* within a time period of *δt*, where *(u, v)* represents the optical flow in two spatial directions (*x* and *y* respectively). The brightness at point *(x, y)* at time *t* is denoted as *I(x, y, t)*. Therefore the brightness constancy equation will be,

$$I(x,y,t) = I(x+u\delta t, y+v\delta t, t+\delta t) \quad (12)$$

For a small pixel motion (say, 1 pixel) and less value of *δt* ($\delta t \to 0$), the above equation (12) can be reduced into the form [8],

$$I_x u + I_y v + I_t = 0 \quad (13)$$

where, $I_x = \frac{\partial I}{\partial x}$, $I_y = \frac{\partial I}{\partial y}$ and $I_t = \frac{\partial I}{\partial t}$ are the partial derivatives of image brightness (intensity) with respect to *x*, *y* and *t*. $u = \frac{dx}{dt}$ and $v = \frac{dy}{dt}$ denote the optical flow velocities. This is limited because only one equation (equation 13) contains two unknown variables and it suffers from aperture problem [9]. To mitigate this challenge, pyramidal refinement of Lucas – Kanade algorithm is approached for determining flow trajectory of air embolus.

2.3.1 Lucas – Kanade Optical Flow and its pyramidal representation

Simple Lucas and Kanade method obtains a velocity optimization by least square estimation principle [9]. The baseline assumption in this case is, the neighboring points of specific object point vary smoothly and posses exactly the same velocity [10]. The brightness constancy equation (13) can be represented in matrix format as,

$$\nabla I^T U = -I_t \quad (14)$$

where, $\nabla I = \begin{bmatrix} I_x & I_y \end{bmatrix}^T$ and $U = \begin{bmatrix} u & v \end{bmatrix}^T$. Therefore, the least square estimation of the error function can be written as,

$$\xi(u,v) = \sum\sum \left[I(x+\delta x, y+\delta y, t+\delta t) - I(x,y,t) \right]^2 \quad (15)$$

Assuming the displacement is small and approximately constant within the neighborhood of an object point, Taylor expansion of $I(x+\delta x, y+\delta y, t+\delta t)$ will be,

$$I(x+\delta x, y+\delta y, t+\delta t) = I(x,y,t) + u\frac{\partial I}{\partial x} + v\frac{\partial I}{\partial y} + \frac{\partial I}{\partial t} \quad (16)$$

Substituting this expression in equation (15) will give,

$$\xi(u,v) = \sum\sum \left[uI_x + vI_y + I_t \right]^2 \quad (17)$$

Now, the optimized value of flow velocities will be achieved by minimizing this error function with respect to *u* and *v*. This will lead to a system of linear equations, matrix representation of which will produce following standard form of Lucas – Kanade optical flow equation [9].

$$U = E^{-1} d \quad (18)$$

where, $E = \begin{bmatrix} \sum\sum I_x^2 & \sum\sum I_x I_y \\ \sum\sum I_x I_y & \sum\sum I_y^2 \end{bmatrix}$ and $d = -\begin{bmatrix} \sum\sum I_x I_t \\ \sum\sum I_y I_t \end{bmatrix}$.

The algorithm for Lucas – Kanade optical flow technique is described below.

Algorithm: Lucas – Kanade Optical Flow

Input: Pair of images *I* and *J* (successive time frames).
Output: Optical flow velocities *(u, v)* of each contour point.
Begin:
Initialize *u* = 0 of size of *I*, and *v* = 0 of size of *J*;
Define the size of *integration window*;
Compute the spatio-temporal derivatives I_x, I_y and I_t;
Set the value of *halfwindow* to floor of (*integration window*/2);
for *i* = (*halfwindow*+1) to (number of rows in I_x – *halfwindow*) with step of 1
  for *j* = (*halfwindow*+1) to (number of columns in I_x – *halfwindow*) with step of 1
    Set the window size,
    Row = i-halfwindow to *i+halfwindow*;
    Column = j-halfwindow to *j+halfwindow*;
    Select the windowed region within I_x, I_y and I_t,
    $tempI_x = I_x$ *(Row, Column)*;
    $tempI_y = I_y$ *(Row, Column)*;
    $tempI_t = I_t$ *(Row, Column)*;
    Take the transpose,
    $tempI_x = (tempI_x)^T$;
    $tempI_y = (tempI_y)^T$;
    $tempI_t = (tempI_t)^T$;
    Set, $tempI_t = -(tempI_t)$;
    Compute an intermediate matrix *A*,
    A = [$tempI_x$ $tempI_y$];
    Determine, $d = A^T \times (tempI_t)$;
    Compute structure tensor matrix, $E = A^T A$;
    Calculate the optical flow velocity, $U = E^{-1} d$;
    Assign, *u(i,j) = U(1)* and *v(i,j) = U(2)*;
  end
end
End.

However, such procedure shows erroneous results in case of large motions (more than 1 pixel). Other hand, selecting a proper integration window is problematic and it depends on the measure of intensity flow (large or small) of the input image. Small window helps to retain the details in the image, but cannot handle large motions. In contrast to this, larger window size is preferable for large motions, but wrongly tracks the motion due to presence of multiple components within window region. Building a pyramidal structure of the images is a solution to this trade off. Pyramid model is structured by low pass filtering and sub-sampling images by a factor of 2, of the preceding layer of the pyramid. Filtering helps to overcome the aliasing effect that can arise during sub-sampling the images [10]. The ground image in such pyramid is the highest resolution image ($I^0 = I$), having original size of

$m \times n$. In the next of pyramid, I^1 is computed from I^0 by first filtering and then sub-sampling I^0 by a factor of 2. Therefore the size of I^0 becomes $(m/2) \times (n/2)$. Then I^2 is computed from I^1 and so on. Let, I^L denotes the image at generic level L ($L = 0, 1, 2, \ldots n$). This way a pyramidal structure is formed with a set of images having gradual decrement in resolution, as we approach towards the highest generic level. Larger pixel motions in base level image become smaller as we approach to the higher level of pyramid due to reduce in image resolution.

Lukas – Kanade optical flow is executed first in the highest level of pyramid using an initial guess of zero for the flow field. Computed optical flow velocity at the highest pyramid level ($L = n$) is then resized by a factor of 2 and propagated to the lower level ($L = n-1$), as initial guess for computing flow velocity in the lower level. This process rolls on up to the ground generic level ($L = 0$). Larger pixel motions can be rightly estimated with small integration window through this approach; hence the problem with the classical method can be resolved.

3. RESULTS AND DISCUSSION

Tracking the air bubble has been performed on the raw speckle images in a fully automated way from pre-processing of speckle images, through segmentation of the emboli in the micro-channel, the optical flow based motion field estimation. The overall programming part has been carried out in MATLAB environment (version 7.10.0). A 3X3 median filter is convolved with the input raw speckle image. Though it successively reduces the background noise (salt and pepper) level, but also the AOI gets blurred. It is then contrast enhanced to brighten the intensities in AOI. Also, dithering has been implemented to improve pixel intensities of AOI by converting the grey levels into binary values. Step-by-step results and their elaborations have been illustrated in the following part.

3.1 Embolus Segmentation

Segmentation has been performed on the dithered image in order to achieve the actual bubble contour within the channel. Conventional AD by Perona and Malik [15] is implemented first over the dithered image. A Gaussian kernel is used to smooth intra-region details while the edge information remains in the output. A 2D network structure of 8 neighboring nodes is considered for diffusion conduction. This results in a rough picture of the actual bubble boundary which is further used as the initial boundary tracking position. The initial positions of the seed contour points are transformed into polar co-ordinate system first to facilitate the programming of AC. The centre is fixed at the centroid of seed contour. Quantization step size for angel θ is $\theta_s = 1°$ (n = 360) and for ρ is ρ_s = 1 pixel. The weighting parameters of different energy functions are kept to be constants as a = 1, b = 0.8, c = d = 0.5. The length of radial direction (R) for computing image energy is chosen small (R = 3) for detecting sharp edges. For calculating grow energy, the intensity in each iteration has been computed over 3x3 pixel (size of k) block. It should be small for tracking local minima or boundaries. Here, e and T value has been taken -0.8 and 20 respectively.

Figure 3 shows detected seed contour after application of AD filtering and its AC counterpart.

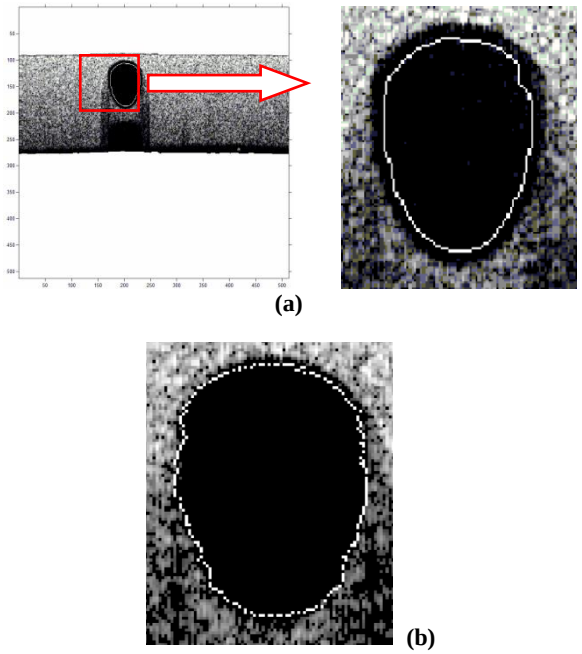

(a) **(b)**

Figure 3. (a) Seed Contour of the embolus after AD, and (b) segmented embolus after AC implementation.

3.2 Segmentation Accuracy

Evaluation of the segmentation process has been performed by measuring segmentation accuracy at the output of the AC technique with respect to a ground truth. Mathematical expression for segmentation accuracy is presented in equation 19.

$$Segmentation\ Accuracy = 1 - \frac{abs(A-B)}{B} \times 100\,\% \qquad (19)$$

Where, A represents the segmented area computed using proposed mechanism and B is the ground truth. It has been experimented that segmentation accuracy falls in the region of 92% – 94%, thereby reflecting a high efficiency in extracting embolus within microchannel.

3.3 Motion Estimation

In The segmented out contour shows the actual position of the air bubble within the channel and over a successive number of time frames it resembles the bubble motion. Motion tracking of the contour points is performed over 40 numbers of time-frames taking at a rate of 20 fps.

Pyramidal Lucak – Kanade technique facilitates the tracking of large pixel motions. Building the pyramid helps to reduce the resolution of the images. This will in turn makes the larger displacements to small pixel displacement and it can be easily tracked down by a small window size. A Gaussian pyramid has been formed to provide more weightage to the centre pixel, by filtering the image with a Gaussian mask and then resize by a factor of 0.5. Here, the pyramid is formed upto a level L = 3, as motion in the ground image limits to 5 – 6 pixels. Integration window size is kept 3×3 and the iteration value is set to 10. Quiver plot of the velocity profile using pyramidal Lucas – Kanade approach is depicted in figure 4. Most of the directional vectors in figure 4 are align to the actual flow field, thereby reflecting the actual flow path of the

air embolus. Flow vectors, which are making some angle with the horizontal axis, reflect the deformation at the contour points of air bubble while flowing through the channel. The pyramidal approach has been implemented over a number of successive time frames and therefore, the velocity trajectory of the air bubble flowing through the microchannel has been easily tracked.

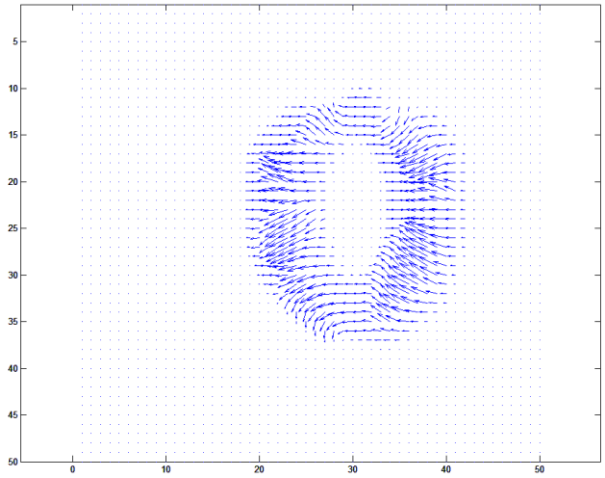

Figure 4. Quiver plot of the optical flow field using Pyramidal Lucas – Kanade method

4. Conclusion

This paper showcases a detailed computerized diagnostic approach for tracking the motion of air embolus in OCT contrast imaging. AD based seed contour initialization helps to minimize manual labor for seed contour detection. An improved snake based AC implementation not only reduces the computational time, but also enhances the boundary tracking ability. The proposed mechanism substantially increases the segmentation accuracy (92% – 94%) for automatic detection of the embolus within the channel. Besides, pyramidal approach of Lucas – Kanade based motion tracking helps in accurate velocity optimization of the air embolus with reasonable computational time. This will facilitate the study of monitoring the flow of air emboli inside the peripheral microvasculature. The proposed approach considers only the air embolism case among different embolism phenomenons. Though this method is limited to the superficial/peripheral regions of the human body, but it can open up a new dimension for diagnosis of peripheral air embolism with minimal invasiveness. This paper also brings out the scopes of contrast imaging with respect to medical image analysis.

5. References

[1] Jain, K. K. 2009 Textbook of Hyperbaric Medicine. Hogrefe & Huber Publishers. 5th edition.

[2] Mirski, M. A., Lele, A. V., Fitzsimmons, L., and Toung, T. J. K. 2007. Diagnosis and treatment of vascular air embolism. J. Anesthesiology. 106. 164–77.

[3] Ward, M. K., Shadforth, M., Hill, A. V. L., and Kerr, D. N. S. 1971. Air Embolism during Haemodialysis. British Medical journal. 3(July 1971). 74-78.

[4] Grosset, D. G., Georgiadis, D,, Kelman, A. W., Cowburn, P., Stirling, S., Lees, K. R., Faichney, A., Mallinson, A., Quin, R., Bone, I., Pettigrew, L., Brodie, E., MacKay, T., and Wheatley, D. J. 1996. Detection of microemboli by transcranial Doppler ultrasound. Texas Heart Institute Journal. 23, 289-292.

[5] Bouma, H., Sonnemans, J. J., Vilanova, A., and Gerritsen, F. A. 2009. Automatic detection of pulmonary embolism in CTA Images. IEEE Trans. on Med. Img. 28 (August 2009). 1223-1230.

[6] McGinn, S., and White, P. D. 1935. Acute cor pulmonale resulting from pulmonary embolism. J. Am. Med. Assoc. 104 (April 1935). 1473-1480.

[7] Juni, J., and Abass, A. 1991. Lung scanning in the diagnosis of pulmonary embolism. In Procedings of Nuclear Medicine. 21. 282-296.

[8] Horn, B. K. P., and Schunk, B. G. 1981. Determining optical flow. Artificial Intelligence 17 (1981). 185-203.

[9] Trucco, E., and Verri, A. 1998. Introductory Techniques To 3d Computer Vision. 1st edition. Prentice Hall. New Jersy.

[10] Fernando, W. S. P., Udawatta, L., and Pathirana, P. 2007. Identification of moving obstacles with pyramidal Lucas – Kanade optical flow and k-means clustering. In Proceedings of the ICIAF 2007. 111-117.

[11] Kearney, K. R., Smith, M. D., Xie, G. Y., and Gurley, J. C. 2006. Massive air embolus to the left ventricle: Diagnosis and monitoring by serial echocardiography. J. Am. Soc. Echo. 10 (December 1997). 982-987.

[12] Hu, M., Ping, X., and Ding, Y. 2004. Automated cell nucleus segmentation using improved snake. In Proceedings of the International Conference on Image Processing.

[13] Kass, M., Witkin, A., and Terzopoulos, D. 1988. Snakes: Active Contour Models. Int. J. Com. Vis. 1(4). 321-331.

[14] Ebrahimdoost, Y., Dehmeshki, J., Ellis, T. S., Firoozbakht, M., Youannic, A., and Qanadli, S. D. 2010. Medical image segmentation using active contours and a level set model: application to pulmonary embolism (PE) segmentation. In Proceedings of the Fourth International Conference on Digital Society.

[15] Perona, P., and Malik, J. 1990. Scale-space and edge detection using anisotropic diffusion. IEEE Trans. Patt. Ana. And Mach. Intelli. 12(7). 629-639.

[16] Masutani, Y., MacMahon, H., and Doi, K. 2002. Computerized detection of pulmonary embolism in spiral CT Angiography based on volumetric image analysis. IEEE Trans. Med. Img. 21(December 2002). 1517-1523.